Drosophila twinfilin is required for cell migration and synaptic endocytosis

Dan Wang[1], Lijun Zhang[2], Guoli Zhao[1], Gudrun Wahlström[3,*], Tapio I. Heino[3], Jiong Chen[2,‡] and Yong Q. Zhang[1,‡]

[1]Key Laboratory of Molecular and Developmental Biology, Institute of Genetics and Developmental Biology, and Graduate University, Chinese Academy of Sciences, Datun Road, Chao Yang District, Beijing 100101, China
[2]Model Animal Research Center and MOE Key Laboratory of Model Animals for Disease Study, Nanjing University, Nanjing 210061, China
[3]Institute of Biotechnology, and Department of Biosciences, University of Helsinki, FIN-00014 Helsinki, Finland
*Present address: Department of Pathology, University of Turku, FIN-20520 Turku, Finland
‡Authors for correspondence (yqzhang@genetics.ac.cn; chenjiong@nicemice.cn)

Accepted 15 February 2010
Journal of Cell Science 123, 1546-1556

doi:10.1242/jcs.060251

Summary

Precise actin regulation is essential for diverse cellular processes such as axonal growth, cell migration and endocytosis. *twinfilin* (*twf*) encodes a protein that sequesters actin monomers, but its in vivo functions are unclear. In this study, we characterized *twf*-null mutants in a metazoan for the first time and found that *Drosophila twf* negatively regulates F-actin formation in subcellular regions of rapid actin turnover in three different systems, namely postsynaptic neuromuscular junction (NMJ) synapses, migratory border cells and epithelial follicle cells. Loss of *twf* function results in defects in axonal growth in the brain and border cell migration in the ovary. Additionally, we found that the actin-dependent postsynaptic localization of glutamate receptor GluRIIA, but not GluRIIB, was specifically reduced in *twf* mutants. More importantly, we showed that *twf* mutations caused significantly reduced presynaptic endocytosis at NMJ synapses, as detected using the fluorescent dye FM1-43 uptake assay. Furthermore, electrophysiological analysis under high-frequency stimulation showed compromised neurotransmission in *twf* mutant synapses, confirming an insufficient replenishment of synaptic vesicles. Together, our results reveal that twinfilin promotes actin turnover in multiple cellular processes that are highly dependent on actin dynamics.

Key words: Twinfilin, Actin turnover, Cell migration, Synapse, Endocytosis

Introduction

The dynamic actin cytoskeleton is essential for a wide range of cellular processes, including endocytosis, cytokinesis, axonal growth and motility. The dynamic nature of the actin structure derives from the fact that monomeric globular (G) actin subunits assemble at the barbed ends of filamentous (F) actin, while actin monomers dissociate from the pointed ends of F-actin (Pantaloni et al., 2001; Paavilainen et al., 2004). Under steady-state conditions, actin filaments undergo 'treadmilling', a process in which actin monomers depolymerized from one end of the filament are recycled and polymerized onto the other end, allowing directional growth of actin filaments without changing their length. This treadmilling process occurs much faster, allowing sustained actin filament growth, in such processes as lamellipodial motility during axonal growth and cell migration, and vesicle internalization during endocytosis. This dynamic treadmilling is regulated by a number of molecules, including highly conserved actin-monomer-binding proteins: profilin, actin-depolymerizing factor (ADF, also known as cofilin), cyclase-associated protein (CAP) and twinfilin. Profilin promotes actin polymerization, whereas the latter three proteins promote actin disassembly, inhibit actin polymerization or both (Palmgren et al., 2002; Paavilainen et al., 2004; Winder and Ayscough, 2005).

Twinfilin is a small protein that sequesters actin monomers. It harbors two ADF-H (ADF-homologous) domains. Like ADF/cofilin, twinfilin shows preferential binding to ADP–G-actin and forms a 1:1 complex with G-actin that prevents its assembly into actin filaments in vitro (Goode et al., 1998; Palmgren et al., 2001; Ojala et al., 2002). Twinfilin is highly abundant in yeast and mammals (Palmgren et al., 2001; Vartiainen et al., 2003); it localizes to subcellular regions of rapid actin turnover, such as cortical actin patches in yeast (Goode et al., 1998; Palmgren et al., 2001), lamellipodia in mammalian cells (Vartiainen et al., 2000; Vartiainen et al., 2003) and the ends of actin bundles in developing *Drosophila* bristles (Wahlström et al., 2001). The localization of yeast twinfilin to actin patches depends on both its actin-monomer-binding ability and the presence of barbed-end-capping proteins (Palmgren et al., 2001; Falck et al., 2004).

Recently, it has been reported that yeast twinfilin also interacts with actin filaments and promotes filament severing at low pH in vitro; its severing activity is inhibited by capping protein and phosphatidylinositol (4,5)-bisphosphate [PtdIns(4,5)P_2] (Moseley et al., 2006). Thus, twinfilin might coordinate filament severing and monomer sequestration at sites of rapid actin turnover (Moseley et al., 2006). In addition to F-actin severing, twinfilins from vertebrates, but not from lower organisms, were found to cap the barbed ends of F-actin, with preferential affinity for ADP-bound ends, thus inhibiting the elongation of actin filaments (Helfer et al., 2006; Paavilainen et al., 2007).

Deletion of *twf* in yeast results in mildly perturbed cortical actin patches with increased F-actin staining, defects in the bipolar bud-site selection pattern, and synthetic lethality with certain ADF/cofilin and profilin mutations (Goode et al., 1998; Wolven et al., 2000; Falck et al., 2004). By contrast, overexpression of *twf* in yeast leads to complete depolarization of the actin cytoskeleton and accumulation of cytoplasmic actin bars (Goode et al., 1998).

Journal of Cell Science

Similarly, overexpression of mouse twinfilin gives rise to a decrease in stress fibers and formation of abnormal actin filament structures in cultured cells (Vartiainen et al., 2000). In summary, alterations of twinfilin expression result in abnormal F-actin structures. However, the physiological function of twinfilin in a multicellular organism remains unclear.

Wahlström et al. showed that the *Drosophila* genome encodes a single homologue of yeast and mammalian twinfilins (Wahlström et al., 2001). Phenotypic analysis of a *twf* hypomorphic allele revealed that *twf* is involved in actin-based bristle development (Wahlström et al., 2001). However, there are no reports of studies on *twf*-null mutants in metazoans. Here, we present the first systematic analysis of a *twf*-null mutant in a multicellular organism. *Drosophila twf* nulls are larval lethal with few adult escapers, indicating that it is critical for viability in flies. We provide evidence demonstrating that twinfilin negatively regulates F-actin formation in multiple cellular contexts. More importantly, we report for the first time that twinfilin is required for different cellular processes in neuronal and non-neuronal systems, including axonal growth in the brain, border cell (BC) migration in the ovary and presynaptic endocytosis at neuromuscular junction (NMJ) synapses. We suggest that the various phenotypes observed in disparate cell types or cellular contexts of *twf* mutants are caused by a shared underlying mechanism of disrupted actin dynamics.

Results

Identification of *twf* mutants

EP(3)3701 inserts in the first intron of *twf* and is a strong hypomorphic allele of *twf* (Fig. 1) (Wahlström et al., 2001). This allele is the only *twf* mutation characterized to date in *Drosophila*. To further understand the in vivo functions of *twf*, we generated null *twf* mutants using *P*-element-mediated excision mutagenesis. We recovered 305 independent excision lines. The breakpoints were first identified by PCR and then pinpointed by DNA sequencing. Here, we report two imprecise deletions, *110* and *102*, in which most of the *twf* coding region is deleted (Fig. 1A). In addition to *twf*, the gene encoding dAbi (the *Drosophila* Abelson interacting protein) lies next to the *EP(3)3701* insertion (Fig. 1A). Using northern analysis, Wahlström et al. showed that the *EP3701* insertion does not affect *dAbi* expression at the transcriptional level (Wahlström et al., 2001). To examine whether the *twf* deletions also affect dAbi expression, we performed western blotting to detect dAbi protein levels. Our results showed that dAbi protein levels remained unchanged in all *twf* mutant lines (Fig. 1B). Thus, the *EP* insertion, subsequently referred to as twf^{3701}, and the two imprecise excisions (twf^{110} and twf^{102}) do not affect the adjacent *dAbi* gene and are *twf*-specific mutant alleles. Ubiquitous expression of *twf* small interfering RNA (siRNA) and upstream activating sequence *(UAS)-twf* by *act-Gal4* caused dramatically reduced and increased expression of twinfilin, respectively (Fig. 1B). More importantly, western blotting and immunostaining showed that twinfilin was not detected in the *110* and *102* deletion lines (Fig. 1B,I,J) indicating that these deletions are null alleles of *twf*.

The deletion mutants were larval lethal with very few adult escapers (Table 1). Lethality was rescued to different extents by the expression of *twf* in muscles by *C57-Gal4*, in neurons by pan-neuronal *elav-Gal4* or ubiquitously by *actin-Gal4* using the UAS-Gal4 system (Table 1), indicating that twinfilin is required for the normal development of different tissues, particularly the nervous system. *Drosophila* twinfilin is ubiquitously expressed in embryos and adult ovaries with high enrichment in BCs, and at various developmental stages (Wahlström et al., 2001). However, its expression in the nervous system has not been documented. Here, we report that twinfilin is enriched in the neuronal soma and processes in the larval and adult brain (supplementary material Fig. S1), as well as at peripheral NMJ synapses. Triple labeling of NMJ synapses with anti-twinfilin, the presynaptic membrane marker anti-horseradish peroxidase (anti-HRP) and the postsynaptic

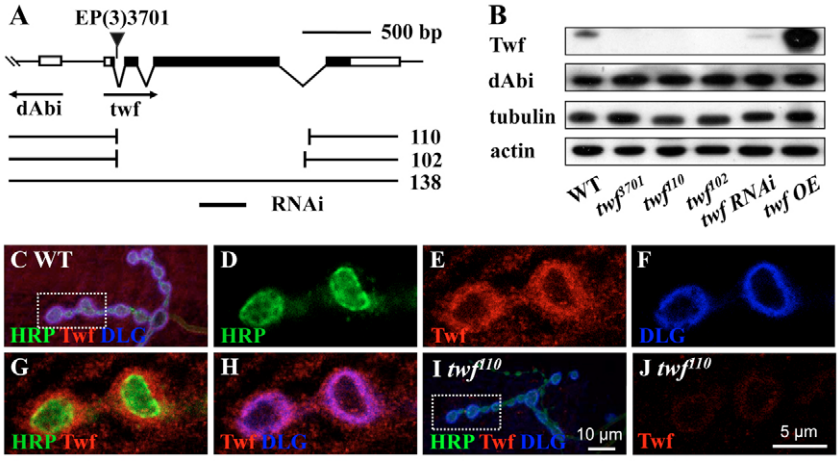

Fig. 1. Identification of *twf* mutants. (**A**) Genomic structure and mutations of *twf*. The insertion site of *EP(3)3701* is indicated. Coding regions are shown as black boxes and non-coding regions are shown as empty boxes. Horizontal arrows indicate the direction of transcription of *dAbi* and *twf*. Shown below are the two intragenic deletions *110* and *102*, and revertant *138* with *twf* intact. The target sequence for the RNAi is indicated. (**B**) Western blotting of adult heads showed that no twinfilin protein was detected in *EP(3)3701* or the two deletion lines *110* and *102*. Significantly decreased and increased expression of twinfilin in the brain was detected in the *twf* RNAi and *UAS-twf* lines, respectively, when they were driven by ubiquitously expressed *act-Gal4*. OE indicates overexpression of *twf* due to induction of *UAS-twf*. Normal expression of *dAbi* occurred in all *twf* mutant flies. Tubulin and actin were used as loading controls. (**C-F**) Twinfilin is enriched at the postsynaptic site of NMJ synapses. NMJ synapses were triple labeled with anti-HRP (a presynaptic membrane marker), anti-twinfilin and anti-Dlg (a postsynaptic marker). (**G**,**H**) Twinfilin is colocalized with postsynaptic Dlg, which surrounds presynaptic HRP. (**I**,**J**) In twf^{110}-null mutants, twinfilin staining was hardly detected at the postsynaptic site. Scale bar: 5 μm.

Table 1. Rescue of *twf* mutant lethality by tissue-specific expression of *twf*

Genotype	Viability (%)	Numbers scored
twf^{102}	1.8	1173
twf^{110}	2.2	554
twf^{102}/twf^{110}	2.2	450
C57-Gal4, twf^{110}*/UAS-twf,* twf^{110}	22	215
elav-Gal4/+;;twf^{110}*/UAS-twf,* twf^{110}	70	300
actin-Gal4, twf^{110}*/UAS-twf,* twf^{110}	100	239

The number of *twf*-null mutants is shown as a percentage of viable adult flies compared to the expected viabilities, which would be half the number of flies carrying a balancer chromosome. Twinfilin is expressed in muscles driven by *C57-Gal4*, in neurons by *elav-Gal4* or ubiquitously by *actin-Gal4* in the *twf*-null background to examine its lethality rescue ability. For each tissue-specific Gal4 line, the percentage of rescued twf^{110} lethality is given.

marker anti-Dlg showed that twinfilin mainly colocalized with postsynaptic Dlg (Fig. 1C-H). Twinfilin staining was hardly detectable at the postsynaptic site in *twf*-null mutants (Fig. 1I,J).

Twinfilin is involved in axonal growth

Precise regulation of actin dynamics is crucial for axonal growth. It has been reported that the actin-monomer-binding proteins ADF/cofilin and Ciboulot (encoded by *cib*), a homologue of β-thymosins with the biochemical properties of profilin, affect axonal growth in the *Drosophila* brain; both *cib* and ADF/cofilin-encoding *tsr* mutants show axonal growth defects (Boquet et al., 2000; Ng and Luo, 2004). To examine a possible role for twinfilin in axonal growth, we examined the neuronal morphology of the mushroom body (MB), for which neuronal development is well documented. Anti-Fas II strongly labels the α and β axonal lobes of the MB (Fig. 2). In wild-type flies, the β lobes terminate near the midline, but rarely grow across it (Fig. 2A). By contrast, 31.4% of the β lobes (n=51) in the twf^{3701} hypomorph crossed the midline and, in severe cases (23.5%), the two β lobes were completely fused (Fig. 2B,C,G). twf^{102} null mutants showed a more severe midline-crossing phenotype (17.5% mild and 35.7% severe; n=40; Fig. 2D,G). The twf^{110} null allele showed phenotypes similar to those of twf^{3701} and twf^{102} (Fig. 2G). Thus, about 50% of the homozygous mutants of the three different alleles had apparent MB midline-crossing defects. The hemizygotes had a weaker but similar phenotype to the homozygotes, suggesting the presence of a background mutation on the mutated chromosomes or a suppressor on the deficiency chromosome (Fig. 2G). However, the midline-crossing phenotype was rescued, at least partially, by the expression of *twf* driven by MB-specific *OK107-Gal4* in the twf^{3701} background (Fig. 2G). Together, these data demonstrate that the axonal midline-crossing phenotype is caused specifically by *twf* mutations. The midline-crossing phenotype in *twf* mutants is similar to that reported for *cib*-overexpressing animals (Boquet et al., 2000).

In addition to the midline-crossing defect, other axonal abnormalities of MB were also observed. In the wild type, individual α/β neurons extend a medial β lobe and a dorsal α lobe from the peduncle (Fig. 2A). By contrast, twf^{102}-null mutants had a missing α lobe, accompanied by thickening of the β lobe (Fig. 2E,F). Either uni- or bi-lateral loss of α lobes occurred with a higher frequency in twf^{102} and twf^{110} null mutants than in hypomorphic twf^{3701} (Fig. 2H). In twf^{102} mutants, 20% of the MBs (n=40) showed unilateral α-lobe loss, whereas 25% of the MBs showed bilateral α-lobe loss. Interestingly, the β lobes were always bifurcated (Fig. 2E) or were much thicker (Fig. 2F) when the

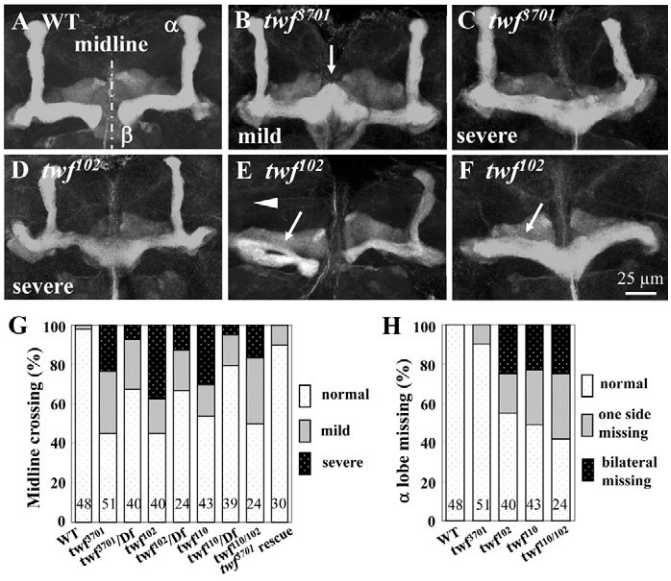

Fig. 2. Twinfilin is involved in axonal growth. (**A-F**) Adult MB lobes are shown by anti-Fas II staining. MB lobes of the *twf* mutants showed axonal midline crossing to various extents. (B) Mild midline crossing was defined as the two β lobes being in close contact or incompletely fused, indicated by an arrow. (C,D) A severe phenotype was defined as the two lobes from each side completely and smoothly fused together. (E,F) *twf* mutants also showed unilateral or bilateral loss of the α lobe (arrowhead) and bifurcated and thickened β lobes (arrows). Scale bar: 25 μm. (**G**) About 50% of the homozygous mutants showed midline crossing; this phenotype was rescued by expression of *twf* driven by *OK107-Gal4* in the twf^{3701} mutant background. Df stands for *Df(3R)suHw*^{7}. (**H**) The percentage of α-lobe missing in different genotypes. The number of animals examined for each genotype is indicated.

ipsilateral α lobe was missing. One possibility for the bifurcated or thickened β lobes is that the α lobe projects parallel to its ipsilateral β lobe, or that the α and β lobes fail to branch at the base of the peduncle, thus forming thickened β lobes instead. These data together show that *twf* regulates axonal growth and guidance.

twf mutants display excessive F-actin formation in multiple cellular contexts

As shown above, twinfilin is enriched at the postsynaptic site (Fig. 1C-J). It has been established that F-actin is also enriched at the postsynaptic site. Postsynaptic F-actin can be best visualized using fluorescently conjugated phalloidin by means of thin (0.4 μm) confocal sectioning (Coyle et al., 2004; Chen et al., 2005). To test whether twinfilin regulates the formation of F-actin, we examined the level of F-actin at the postsynaptic site in the wild type and *twf* mutants (Fig. 3A,B). In wild-type larvae, postsynaptic F-actin surrounded presynaptic boutons, whereas in twf^{110} null mutants, a markedly increased level of F-actin was observed, using anti-HRP staining as an internal control (compare Fig. 3B with 3A), even though the NMJ morphology was normal. Statistical analyses showed that twf^{110} mutants had significantly increased phalloidin-staining intensity compared with the wild-type controls (Fig. 3D; 135.6±3.2 for mutants versus 100±1.8 for wild type; n=8; P<0.001). Conversely, when *twf* was overexpressed postsynaptically by muscle-specific *C57-Gal4*, the F-actin level showed a significant 17% reduction in staining intensity compared with the wild type (P<0.001; Fig. 3D).

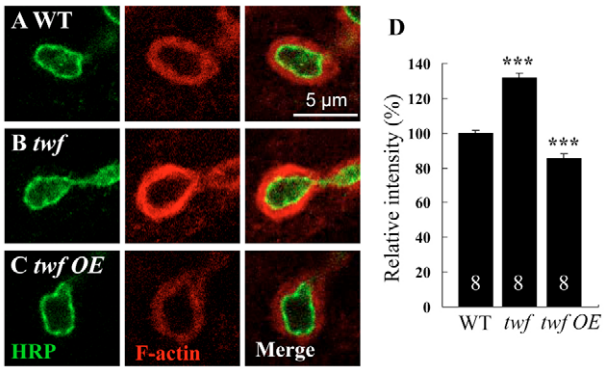

Fig. 3. Twinfilin negatively regulates F-actin formation at the postsynaptic site. (**A-C**) NMJ synaptic boutons were double stained with anti-HRP (green) and phalloidin (red). Anti-HRP labels presynaptic membranes. Phalloidin labels F-actin. (A) Wild-type (WT). (B) *twf*^{110} mutant. (C) Overexpression of *twf* in postsynaptic muscles by *C57-Gal4* (*twf* OE). Scale bar: 5 µm. (**D**) Quantification of fluorescence intensity. The number of animals analyzed for each genotype is indicated. ***P<0.001; error bars indicate s.e.m.

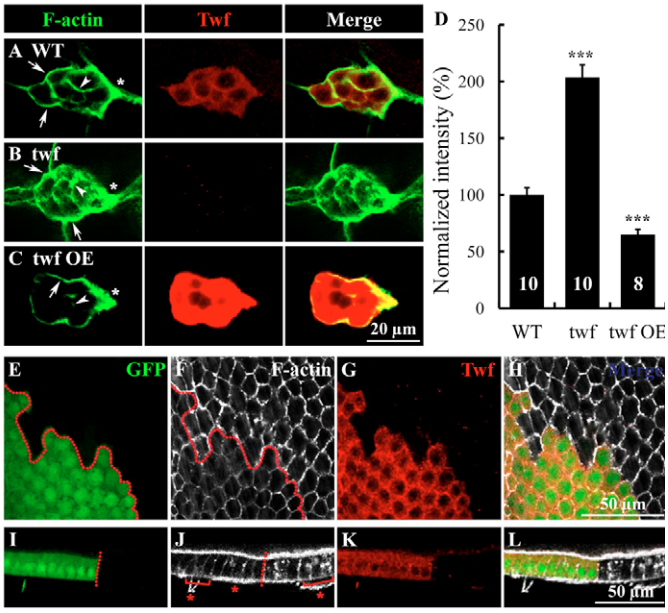

Fig. 4. Twinfilin negatively regulates F-actin formation in BCs and follicle cells. (**A-C**) Representative images of BC clusters from different genotypes stained with phalloidin (green) and anti-twinfilin (red). Images for different genotypes were collected at identical settings. The arrowhead marks the cell-cell contacts within the BC cluster and the arrows point at the outline of a cluster where BCs contact nurse cells. The asterisk indicates the lamellipodial protrusion of the leading edge. (**D**) Quantification of the F-actin staining intensity. *twf*^{3701} mutants displayed increased levels of F-actin, whereas *twf* overexpression (*twf* OE), driven by BC-specific *slbo-Gal4*, led to a decrease in F-actin staining compared with the wild type. The number of egg chambers analyzed for each genotype is indicated. ***P<0.001; error bars indicate s.e.m. (**E-H**) The level of F-actin is increased in the cortical region of mutant follicle cell clones in a planar view. (**I-L**) In a cross-section view of the follicle epithelium, increased F-actin staining was observed at the lateral and apical but not the basal regions of the mutant cells. Apical is up; basal is to the bottom. Red brackets mark regions of the basal cortex of follicle cells in both the mutant and wild type that are not covered by pieces of muscular sheath (indicated by asterisks) attached to the egg chamber. *twf*^{110} mutant clones in E to L are indicated by the absence of both GFP (E and I) and twinfilin staining (G and K). Scale bar: 50 µm.

To further understand the role of twinfilin in regulating F-actin formation, we examined the level of F-actin in the cluster of 6-10 migratory BCs where twinfilin is highly expressed (Fig. 4A) (Wahlström et al., 2001). Twinfilin is mainly cytoplasmic, whereas F-actin is localized to the cortical region of the BCs and is highly enriched in the periphery of the BC cluster (Fig. 4A). Statistical analysis showed that the *twf*^{3701} mutation resulted in a twofold increase in F-actin staining intensity in the BCs (203.5±11.1 in *twf* mutants versus 100±6.2 in wild type; n=10 for both; P<0.001; Fig. 4D). Conversely, overexpressing *twf* in BCs by *slbo-Gal4* resulted in a significant 35% decrease in the F-actin level (P<0.001; Fig. 4D).

In addition to the mutant analysis, we also performed mosaic analysis to better examine the role of twinfilin in F-actin formation. As *twf* is highly expressed in the large, single layer of follicle cells of a developing egg chamber (Wahlström et al., 2001), where the effect of actin regulators such as profilin and cofilin on F-actin formation has been well studied (Baum and Perrimon, 2001), we generated mitotic clones mutant for *twf*^{110} in the follicle cells. Cells from a planar section in *twf*^{110} mutant clones exhibited a significant increase in the F-actin level compared with the adjacent wild-type cells (Fig. 4E-H). To better reveal F-actin misregulation in *twf* mutants, we analyzed F-actin staining in a cross-section of the epithelial follicle cells (Fig. 4I-L). An obvious increase in F-actin was largely limited to the apical surface and lateral junctions, but not to the basal regions of the *twf*^{110} mutant follicle cells (Fig. 4I-L), consistent with the increased F-actin level in the planar view (Fig. 4F). Increased F-actin was also observed in *twf*^{110} mutant clones in eye disc epithelial cells (supplementary material Fig. S2). Taken together, both mutant and clonal analyses demonstrate that *Drosophila* twinfilin negatively regulates F-actin formation in multiple cellular contexts.

twf is required for border cell migration

We have previously shown that ADF/cofilin suppresses F-actin formation and is required for BC migration (Chen et al., 2001). Because both twinfilin and ADF/cofilin suppress F-actin formation, we then tested whether twinfilin also plays a similar role in BC migration. The BCs in stage 9 egg chambers migrate as a cluster between the nurse cells and eventually reach the border between the nurse cells and the oocyte by early stage 10. The stereotypic migration of BCs can be easily quantified; thus, it serves as an excellent model for evaluating the role of a gene in cell migration. It was previously reported that hypomorphic *twf*^{3701} displays no obvious defects in BC migration at 25°C (Wahlström et al., 2001), which we have confirmed. However, we detected a moderate but significant delay in BC migration in both *twf*^{3701} homozygous and *twf*^{3701}/*twf*^{110} heteroallelic mutants when they were cultured at 29°C, a suboptimal temperature for fruit flies (Fig. 5H). Targeted overexpression of *twf* in BCs by BC-specific *slbo-Gal4* at 29°C showed a mild migration delay (Fig. 5H), indicating that an apparent reduction in F-actin levels in the BC cluster does not have an obvious effect on BC migration. However, *twf* RNAi knockdown under identical conditions resulted in a significant migration delay: 48% of the BC clusters examined failed to reach the border, whereas only 4% of the BC clusters in GFP control animals had yet to reach their destination (Fig. 5H). In the overexpression and RNAi knockdown assays, transgenic flies were cultured at 29°C

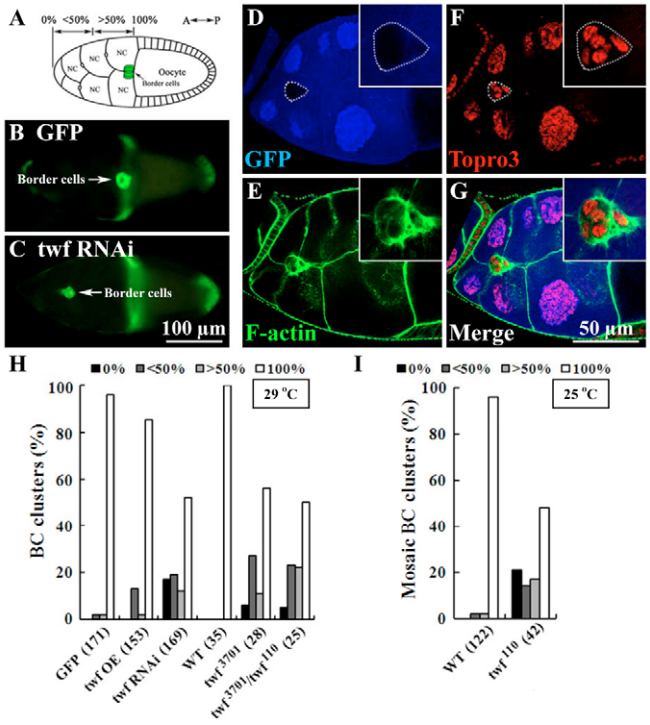

Fig. 5. *twf* is required for BC migration. (**A**) Schematic diagram of a stage 10 egg chamber. BCs (green) and the anterior-posterior axis are indicated. NC denotes nurse cell. The positions of BCs during migration are graded as 0% (starting point for migration), <50%, >50% and 100% (final destination, i.e. the border). (**B**) BCs expressing GFP as the wild-type control and (**C**) *twf* siRNA driven by *slbo-Gal4* with a migration delay. (**D-G**) A migration-delayed BC cluster at the 25% position. All the BCs are twf^{110} mutant without GFP (D). The mutant clone is shown at higher magnification in the inset. Nuclei are labeled by Topro3 and F-actin is stained by phalloidin. Scale bar: 50 μm. (**H**,**I**) Quantification of BC migration in different genotypes. BC positions are indicated by vertical bars with different shades. Overexpression (OE) and RNAi knockdown by *slbo-Gal4* were induced at 29°C for a stronger effect due to higher expression of Gal4 (H). BC migration was examined for twf^{3701} homozygous and twf^{110}/twf^{3701} mutants cultured at 29°C (H). twf^{110} mutant clones also show a migration delay at 25°C (I). The number of BC clusters examined for each genotype is indicated within parentheses.

for a stronger effect due to higher expression of Gal4 at that temperature. Similarly, twf^{110} mitotic clones in the BC clusters also resulted in a migration delay at 25°C: 52% of the BC clusters containing twf^{110} mutant clones displayed a migration delay, whereas 96% of the wild-type BC clusters reached their final destination (Fig. 5I). These results together demonstrate an essential role for *twf* in BC migration.

twf specifically regulates the postsynaptic expression of glutamate receptor GluRIIA

It has been demonstrated that the actin cytoskeleton plays a role in the postsynaptic membrane localization of glutamate receptors (GluRs). This modulates the postsynaptic response to neurotransmitters (Shirao and Sekino, 2001; Coleman et al., 2003; Chen et al., 2005). Two subtypes of GluRs are characterized by the presence of either the GluRIIA or GluRIIB subunit, together with shared GluRIIC, GluRIID and GluRIIE subunits (Chen et al., 2005). The A- and B-type receptors have functional differences and are spatially segregated as homotypic clusters (DiAntonio et al., 1999; Marrus et al., 2004). In mammals, extensive studies have shown that GluRs cluster at postsynaptic sites through interactions with the actin cytoskeleton (Rosenmund and Westbrook, 1993; Shirao and Sekino, 2001; Coleman et al., 2003).

We investigated whether actin-mediated GluR localization at the postsynaptic site was disrupted in *twf* mutants. As shown in Fig. 6, GluRIIA levels were mildly but significantly decreased in *twf*-null mutants (77.8±2.0; n=12; P<0.001) compared with the wild type (100±3.1; n=12). By contrast, GluRIIB levels remained the same in *twf* mutants (96.9±2.7; n=12; P>0.1) as in the wild type (100±2.6; n=12; Fig. 6B,D). To ascertain whether the decreased levels of GluRIIA in *twf* mutants were specifically due to the absence of twinfilin, we examined the expression of GluRs when *twf* was expressed by muscle-specific *C57-Gal4* in the *twf* mutant background. Expression of *twf* postsynaptically rescued the decreased GluRIIA level in the *twf* mutants (96.2±2.4; n=6; P>0.1), although the level of GluRIIB was mildly but significantly reduced (88.9±3; P<0.05; Fig. 6C,D). These data demonstrate that *twf* regulates the postsynaptic expression of glutamate receptor GluRIIA in a subtype-specific manner.

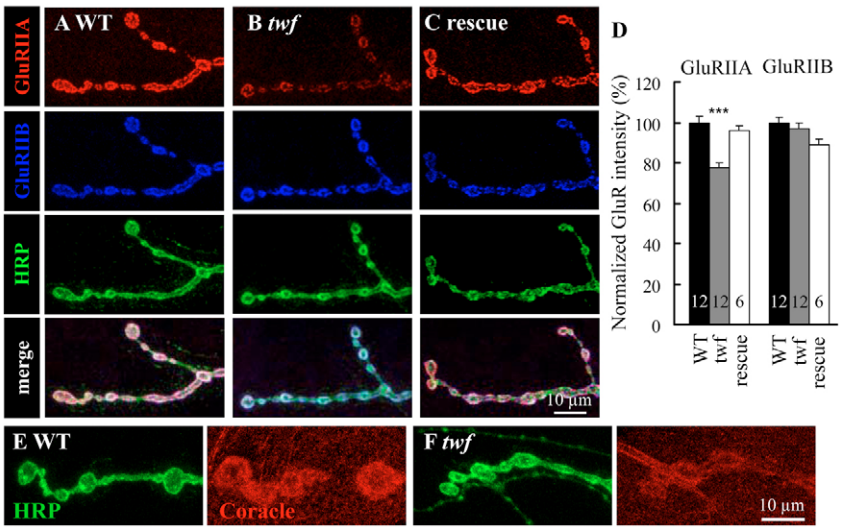

Fig. 6. The postsynaptic abundance of GluRIIA is specifically reduced in *twf* mutants. (**A-C**) Representative images of NMJ synapses stained with anti-GluRIIA (red), anti-GluRIIB (blue) and anti-HRP (green) from the wild type, twf^{110} mutants and twf^{110} mutants expressing *twf* postsynaptically (rescue). Scale bar: 10 μm. (**D**) Relative fluorescence intensities of GluR staining. The fluorescence intensity of the wild type was normalized as 100. The number of animals analyzed is indicated. ***P<0.001; error bars indicate s.e.m. (**E**,**F**) Coracle was significantly reduced in twf^{110}-null mutants compared to the wild type. Scale bar: 10 μm.

GluRIIA was reported to be anchored to F-actin at NMJ synapses through Coracle, the *Drosophila* homologue of actin-interacting 4.1 protein (Chen et al., 2005). To test whether Coracle expression at NMJ synapses was altered in *twf* mutants, we stained NMJ synapses with guinea-pig anti-Coracle. The intensity of anti-Coracle staining was significantly reduced by 30% in twf^{110} mutants compared with the wild type (n=10; P<0.001; Fig. 6E,F), suggesting that the reduced GluRIIA in *twf* mutants might be caused by decreased Coracle.

Endocytosis but not exocytosis is impaired in *twf* mutants

In yeast, *twf* mutants have no defects in fluid-phase marker uptake (Goode et al., 1998). However, in cultured mammalian cells, the subcellular distribution of endocytic organelles is disrupted when *twf* is knocked down (Pelkmans et al., 2005); expression of either the N- or the C-terminal ADF-H domain of mouse twinfilin leads to decreased efficiency of transferrin uptake (Helfer et al., 2006). These data indicate that twinfilin might be involved in endocytosis and in actin-driven internalization or mobility of endocytic vesicles in metazoans. However, a possible role for twinfilin in endocytosis at the multicellular organism level has not yet been tested.

To examine whether endocytosis at NMJ synapses is affected in *twf* mutants, we performed fluorescent dye FM1-43 uptake experiments. FM1-43 can be taken up in synaptic vesicles by endocytosis and released by exocytosis. Compared to the wild-type controls, which displayed intense labeling of FM1-43 at synaptic boutons (the revertant *138* also showed synaptic loading of FM1-43 comparable to that of the wild type, data not shown), *twf*-null mutants showed a significantly reduced amount of loaded dye (Fig. 7). The relative fluorescent intensity of *twf* mutants was ~60% of that of the wild-type controls (n=8; P<0.001; Fig. 7A,B,G). Correspondingly, the amount of remaining dye in the mutants after unloading triggered by high K^+ stimulation was also reduced compared with that in the controls (P<0.01; Fig. 7C,D,G). However, the ratio of unloaded to loaded FM1-43 showed no difference between *twf* mutants and wild-type controls, indicating that exocytosis is not affected (Fig. 7H). The decrease in the amount of loaded and unloaded FM1-43 dye in *twf* mutants was largely rescued by presynaptic expression of *twf* by *elav-Gal4* (Fig. 7G). These results indicate that *twf* is involved specifically in endocytosis but not in exocytosis.

As shown above, *twf* mutants show increased F-actin formation (Figs 3 and 4; supplementary material Fig. S2). To further understand whether the endocytosis defect in *twf* mutants is caused by the increased F-actin level, we examined endocytosis after pharmacological disruption of the actin cytoskeleton. We treated NMJ synapses before FM1-43 dye uptake with a low concentration (0.1 μM) of latrunculin A (LatA), which promotes actin depolymerization by sequestering G-actin. The relative amount of loaded FM1-43 in wild-type synapses was significantly reduced compared with the untreated controls (Fig. 7E,I; 21.5±1.3 in *twf* mutants versus 100±4.1 in the wild type; P<0.001). By contrast, LatA treatment of the *twf* mutants showed no significant effect on endocytosis (Fig. 7F,I; 61.1±6.6 for LatA treated versus 61.7±6.6 for untreated; P>0.05). However, when treated with a high concentration of LatA (10 μM), endocytosis was completely blocked in both wild-type and mutant animals (data not shown). The pharmacological analysis showed that endocytosis in *twf* mutants is more resistant to LatA treatment at a low concentration of 0.1 μM, consistent with our finding presented above that the levels of F-actin are increased in the *twf* mutants.

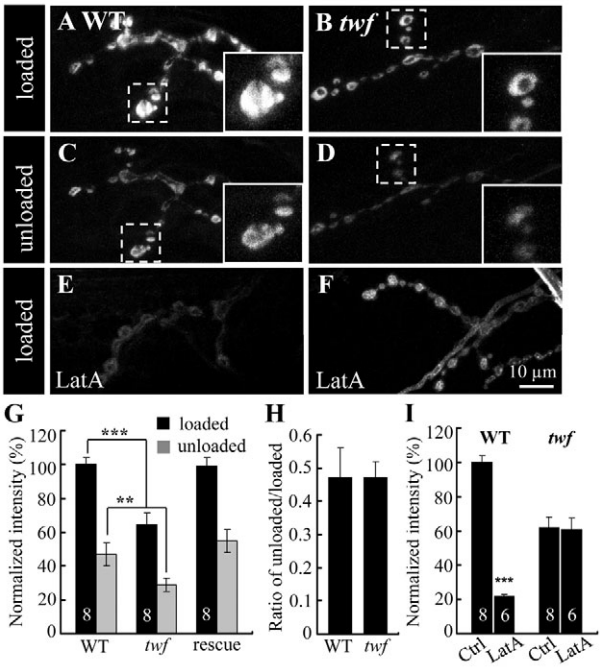

Fig. 7. Loss of *twf* causes synaptic endocytic defects. (**A**,**C**) Wild-type NMJ synapses loaded with FM1-43 and subsequently unloaded by high K^+ saline. (**B**,**D**) Reduced levels of loaded and unloaded FM1-43 dye in twf^{110} mutants compared to the wild type. (**E**,**F**) Disruption of F-actin by LatA impaired dye uptake in wild-type controls, but not in twf^{110} mutants. Scale bar: 10 μm. (**G**) Significantly reduced loaded and unloaded FM1-43 in twf^{110} mutants compared with the wild type. The endocytic defect was rescued by neuronal expression of *twf* driven by *elav-Gal4*. The number of animals analyzed is indicated. (**H**) The ratio of unloaded to loaded FM1-43 showed no alteration in twf^{110} mutants compared with the wild type. (**I**) Fluorescence intensities after pharmacological disruption of F-actin by LatA at 0.1 μM are shown for both wild type and twf^{110} mutants. Ctrl indicates untreated controls. The number of animals analyzed is indicated. ***P<0.001, **P<0.01; error bars indicate s.e.m.

twf mutants show compromised neurotransmission under intense stimulation

To further ascertain whether *twf* is required for endocytosis, we examined synaptic neurotransmission in *twf* mutants using physiological assays. We first recorded the postsynaptic excitatory junctional potentials (EJPs) triggered by nerve stimulation and spontaneous miniature excitatory junctional potentials (mEJPs) without nerve stimulation at NMJ synapses of late third instar larvae. Evoked EJP amplitudes upon low-frequency stimulation of 0.3 Hz in twf^{110} and control animals were similar (Fig. 8A-C; P>0.05). In addition, we evaluated spontaneous neurotransmitter release by analyzing mEJPs. The mEJP amplitudes were not significantly altered in *twf* mutants compared with the wild type (Fig. 8D). The mEJP frequency in homozygous twf^{110} mutants showed a significant decrease (P<0.05), but the decrease in mEJP frequency did not present in twf^{110} hemizygous mutants (P>0.05), suggesting that the phenotype is not caused by the *twf* mutation (Fig. 8E). The quantal content, calculated by dividing the corrected EJP amplitude by the mEJP amplitude, was not altered either (Fig. 8F; P>0.05). Thus, basal transmission upon low-frequency stimulation is not affected in the *twf* mutants.

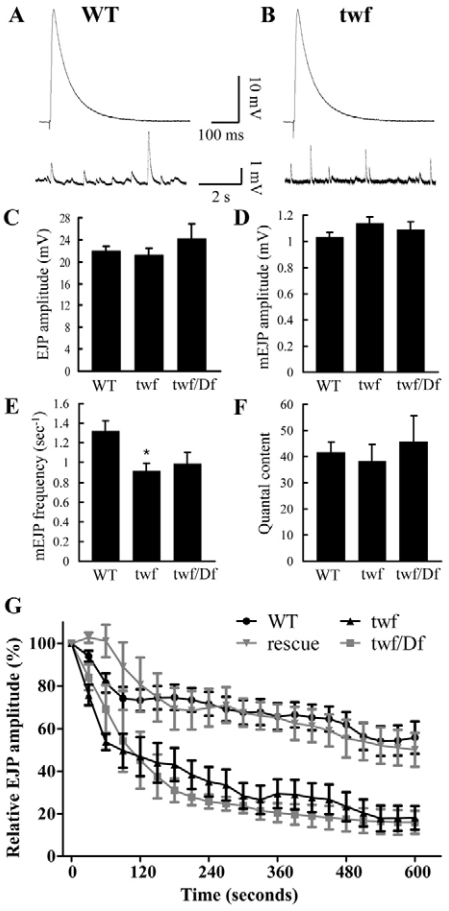

Fig. 8. *twf* mutants fail to sustain neurotransmitter release under tetanic stimulation. (**A**,**B**) Representative traces of EJPs elicited by low-frequency (0.3 Hz) stimulation and mEJPs from wild-type controls and twf^{110} mutants. (**C**-**F**) EJP amplitudes, mEJP amplitudes, mEJP frequencies and quantal content of the wild type (WT), twf^{110} and $twf^{110}/Df(3R)SuHw^{7}$. At least eight animals were analyzed for each genotype. Error bars indicate s.e.m. (**G**) Relative EJP amplitudes during a 10-minute high-frequency (10 Hz) stimulation of different genotypes. The genotypes tested are: WT, twf^{110}, $twf^{110}/Df(3R)SuHw^{7}$ and *elav-Gal4*/+;; twf^{110}/*UAS-twf* twf^{110}. At least six animals were analyzed for each genotype. Error bars indicate s.e.m.

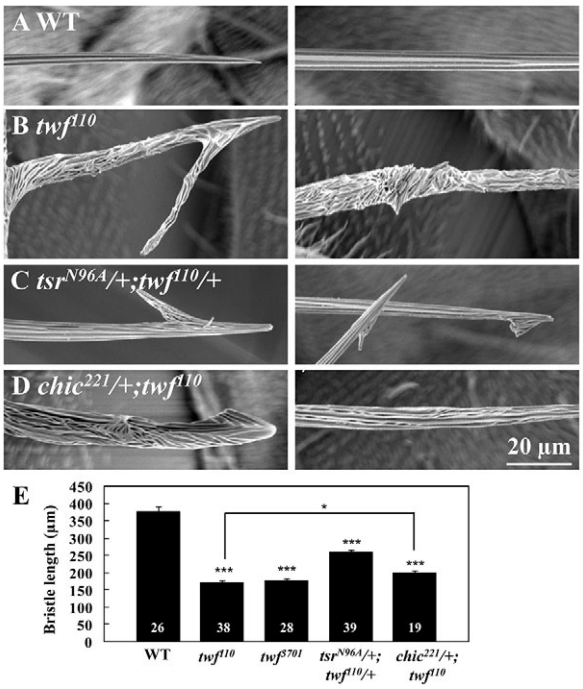

Fig. 9. *twf* and *chic* have an antagonistic effect on actin-based bristle development. (**A**) Wild-type bristles show straight, parallel ridges. (**B**) Bristles of twf^{110} mutants show forked tips and completely disorganized ridges. (**C**) $tsr^{N96A}/+;twf^{110}/+$ transheterozygotes show mildly disorganized ridges and hooked tips. (**D**) The twf^{110} bristle phenotype is partially rescued by the heterozygous $chic^{221}$ mutation. Scale bar: 20 μm. (**E**) twf^{110}, twf^{3701}, $tsr^{N96A}/+;twf^{110}/+$ and $chic^{221}/+;twf^{110}$ showed greatly decreased bristle length compared with wild-type bristles. $chic^{221}$ dominantly and partially rescued the reduced bristle length of twf^{110} mutants. The number within the bar indicates the number of bristles analyzed from >6 animals. ***P<0.001, *P<0.05; error bars indicate s.e.m.

The *twf* mutations impair endocytosis but not exocytosis (Fig. 7), and endocytosis mutants such as *endophilin* and *dap160*/*intersectin* mutants cannot maintain neurotransmission during intense stimulation because of insufficient replenishment of synaptic vesicles (Verstreken et al., 2002; Koh et al., 2004). Therefore, we then examined the EJPs when intense stimulation at 10 Hz was delivered to the nerve for 600 seconds. In control animals, the EJP amplitudes gradually declined to about 60% of the original level within the 600 second stimulation period. By contrast, under the same stimulation regime, the EJP amplitudes detected in the twf^{110}-null mutants dropped sharply in the first 240 second period (Fig. 8G) and reached about 20% of the original level. The hemizygous mutants (twf^{110} over-deficiency) showed a similar phenotype as the homozygous twf^{110} mutants. Furthermore, presynaptic expression of twinfilin driven by *elav-Gal4* completely rescued the enhanced decrease in EJP amplitudes in twf^{110} mutants (Fig. 8G). Together, these data demonstrate that the dramatic reduction in EJPs under high-frequency stimulation, consistent with the defective endocytosis detected by the FM1-43 uptake assay, is caused specifically by *twf* mutations.

twf and *chic* act antagonistically in regulating bristle development and synaptic endocytosis

Yeast *twf*-null mutants are viable, but synthetically lethal in combination with *profilin* or *ADF/cofilin* mutants (Goode et al., 1998; Wolven et al., 2000; Falck et al., 2004). In *Drosophila*, transheterozygotes of *twf* and *tsr*, which encodes ADF/cofilin, show a subtle bristle phenotype reminiscent of that seen in homozygous *twf* mutants (Wahlström et al., 2001), consistent with the fact that both *twf* and *tsr* suppress F-actin formation (Figs 3 and 4) (Chen et al., 2001). To further understand the role of twinfilin in regulating the actin cytoskeleton, we examined the genetic interaction of twinfilin with profilin, which promotes actin polymerization and is encoded by *chic*. Wild-type bristles have smooth, parallel ridges, whereas the bristles of the *twf*-null adult escapers show forked tips and severely twisted ridges (Fig. 9A,B). Bristles of $tsr^{N96A}/+;twf^{110}/+$ transheterozygotes showed mildly disorganized ridges and hooked tips, confirming the previous report (Fig. 9C) (Wahlström et al., 2001). Because profilin promotes F-actin assembly, whereas twinfilin inhibits F-actin formation, we would expect a rescue effect if the amount of profilin is reduced in

the *twf* mutant background. This is indeed the case. Homozygous $chic^{221}$ is embryonically lethal. Double mutants of *twf* and $chic^{221}$ are embryonically lethal, precluding the examination of bristles, whereas reducing profilin by half partially rescued the bristle phenotypes of twf^{410} homozygous mutants (compare Fig. 9D with Fig. 9B). As a control, $chic^{221}$/+;twf^{410}/+ transheterozygotes showed wild-type bristles (data not shown).

In addition, the bristle length of twf^{410} animals is significantly shorter than that of the wild type (Fig. 9E). Statistical analysis showed that the reduced bristle length in *twf* mutants was also partially rescued by reducing *chic* expression by half (177.4±6.7 μm in *twf* mutants and 199.1±8.2 μm in $chic^{221}$/+;twf^{410}; n>19; P<0.05; Fig. 9E). The interaction between *twf* and *chic* is similar to that reported for the interaction between *capping protein* and *chic* (Hopmann and Miller, 2003). Capping protein limits F-actin formation by binding to the F-actin barbed ends.

To further confirm the genetic interaction between *twf* and *chic*, we examined FM1-43 uptake at NMJ synapses and found that the reduced FM dye uptake in twf^{410} mutants was rescued substantially in the double mutants (P<0.01; supplementary material Fig. S3), consolidating the antagonistic effect between the two. The genetic interaction assays indicate that *twf* and *chic* function antagonistically in regulating actin dynamics during bristle development and synaptic endocytosis.

Discussion

twf suppresses F-actin formation and is involved in axonal growth and cell migration

Twinfilin is well established as a protein that sequesters actin monomers (Goode et al., 1998; Wahlström et al., 2001; Helfer et al., 2006). However, its in vivo function remains largely unclear. Our work provides multiple lines of evidence from both mutant and mosaic clone analyses demonstrating that *Drosophila twf* suppresses F-actin formation in subcellular regions of high actin dynamics in multiple cellular contexts, that is, NMJ synapses, migrating BCs and epithelial follicle cells. In *twf* mutants and mutant clones, there is excessive F-actin, whereas overexpression of *twf* leads to reduction in the F-actin level (Figs 3 and 4; supplementary material Fig. S1). In yeast, *twf* mutation also results in enlargement of cortical actin patches (Goode et al., 1998; Moseley et al., 2006). The increase in the F-actin level of *twf* mutant yeast and *Drosophila* is consistent with in vitro studies demonstrating that twinfilin inhibits nucleotide exchange on actin monomers and prevents assembly of the monomer into filaments (Palmgren et al., 2002). It is noteworthy that loss of ADF/cofilin function also results in excessive F-actin in yeast and in *Drosophila* (Lappalainen and Drubin, 1997; Chen et al., 2001). Moreover, genetic interaction assays in *Drosophila* showed that twinfilin acts in the same process as ADF/cofilin, but antagonistically with profilin in actin-based bristle development (Fig. 9) (Wahlström et al., 2001). Thus, our work provides multiple lines of in vivo evidence implicating twinfilin in regulating F-actin formation and actin dynamics.

Twinfilin promotes actin-based motility in an in vitro biomimetic motility assay (Helfer et al., 2006). In S2 cells, RNAi knockdown of twinfilin expands the lamellipodia at the expense of the lamellum (Iwasa and Mullins, 2007). However, its requirement in cellular processes such as axonal growth and cell migration has not been tested. We found that *twf* mutants show overgrown axons in the brain, in contrast to *tsr* mutants (Ng and Luo, 2002), but similar to that reported for *dfmr1* mutants (Michel et al., 2004) and for *cib*-overexpressing animals (Boquet et al., 2000). Cib is an actin-binding protein with a function similar to profilin (Boquet et al., 2000). BC migration in the egg chamber of *Drosophila* is a well-studied cell behavior that is genetically tractable (Naora and Montell, 2005). Many proteins, including the actin-monomer-binding proteins profilin and ADF/cofilin, have been identified to be required for this process (Chen et al., 2001; Naora and Montell, 2005). Our work from mutant and clonal analyses, as well as RNAi knockdown experiments, provides evidence demonstrating, for the first time, that twinfilin is required for BC migration in the developing ovary (Fig. 5).

Twinfilin is required for postsynaptic localization of the specific glutamate receptor GluRIIA

The mechanism by which neurotransmitter receptors are anchored to the postsynaptic membrane is largely unknown. Our immunohistochemical analysis revealed that the post-synaptic expression of GluRIIA, but not GluRIIB, is specifically reduced in *twf* mutants, demonstrating that *twf* regulates GluR localization at synapses in a receptor-subtype-specific manner. Coracle, the fly homologue of mammalian actin-interacting protein 4.1 that binds directly and specifically to GluRIIA (Chen et al., 2005), was also reduced in *twf* mutants (Fig. 6E,F). These results agree well with previous findings that Coracle is required for the proper localization of GluRIIA, but not GluRIIB (Chen et al., 2005). Pharmacological disruption of F-actin phenocopies the *coracle* mutants with reduced GluRIIA expression (Chen et al., 2005). However, in *twf* mutants, there was more F-actin than in the wild type (Fig. 3), but GluRIIA was specifically downregulated, suggesting that the mere presence of F-actin is not sufficient to localize GluRIIA correctly. As twinfilin is conserved throughout evolution and actin regulates the postsynaptic localization of mammalian GluRs (Coleman et al., 2003; Cingolani and Goda, 2008), we predict a similar role for twinfilin in mammals.

Twinfilin is required for presynaptic endocytosis

Although yeast *twf*-null mutants have no defects in endocytosis (Goode et al., 1998), mammalian twinfilin is involved in clathrin-mediated endocytosis and redistribution of endocytic organelles in cultured cells (Pelkmans et al., 2005). Overexpression of either the N- or the C-terminal ADF-H domain of mammalian twinfilin in cultured cells also results in defects in receptor-mediated endocytosis (Helfer et al., 2006). Consistent with the studies in cultured cells (Pelkmans et al., 2005; Helfer et al., 2006), our phenotypic analyses of *Drosophila* mutants demonstrate, for the first time, that twinfilin is required for presynaptic endocytosis in vivo (Figs 7, 8), even though it is enriched at the postsynaptic site (Fig. 1). First, *twf* mutants had endocytic defects at NMJ synapses, as shown by the FM1-43 uptake assay (Fig. 7A-D,G). Second, pharmacological disruption of F-actin by LatA at a low concentration of 0.1 μM in the wild type caused endocytic defects, but had little effect on endocytosis in *twf* mutants (Fig. 7E-F,I), consistent with the presence of increased F-actin levels in *twf* mutants (Figs 3, 4). Third, the EJP amplitude dropped precipitously in the *twf* mutant synapses under intense stimulation (Fig. 8G), whereas the basal transmission is normal (Fig. 8A-F), indicating an inability to retrieve synaptic vesicles. Last, endocytic protein AP180, but not other synaptic proteins such as α-adaptin, Eps15 and EndoA, was mildly but significantly reduced at NMJ synapses in *twf* mutants by immunostaining (supplementary material Fig. S4). Collectively, our data demonstrate that *Drosophila* twinfilin is

required for endocytosis. It has been well established that a highly dynamic actin cytoskeleton is essential for endocytosis (Kaksonen et al., 2006; Smythe and Ayscough, 2006). However, the mechanism by which *twf* regulates endocytosis is currently unknown. One simple explanation is that the increased level of F-actin in the *twf* mutants hinders the actin-driven internalization or mobility of endocytic vesicles. Alternatively, the endocytosis defects in *twf* mutants could be caused by misregulation of the endocytic protein AP180.

Interestingly, mutants of endocytic genes such as *endophilin*, *synaptojanin*, *dynamin* and *AP180* all show dramatic increases in the number of satellite boutons at NMJ synapses (Dickman et al., 2006). Similarly, mutations in other actin regulators, such as CYFIP (cytoplasmic FMRP interacting protein), WASP (Wiskott-Aldrich syndrome protein) and Nwk (nervous wreck), also exhibit prominent defects in synaptic growth (Schenck et al., 2003; Coyle et al., 2004). As shown in this study, twinfilin is involved in endocytosis and negatively regulates F-actin formation. However, the NMJ synapses in *twinfilin* mutants examined by immunostaining displayed no obvious morphological abnormalities (data not shown), demonstrating that, in contrast to endocytic proteins and the other actin regulators, twinfilin is not essential for synapse growth, but rather is involved in specific synaptic functions, that is, postsynaptic localization of glutamate receptors and presynaptic endocytosis. The mechanism by which *twf* functions at synapses, as related to endocytic proteins such as AP180 and the other actin regulators, remains to be elucidated.

Like twinfilin, other actin-monomer-binding proteins, such as ADF/cofilin and profilin, are also essential for endocytosis in both yeast and mammalian cells. ADF/cofilin, which promotes F-actin depolymerization, is required for endocytosis and membrane trafficking to the vacuoles in yeast (Lappalainen and Drubin, 1997; Idrissi et al., 2002; Okreglak and Drubin, 2007). Profilin, which promotes F-actin polymerization, has the opposite effect to ADF/cofilin on endocytosis in cultured cells (Gareus et al., 2006). Loss of mouse brain-specific profilin 2 results in increased endocytosis, whereas its overexpression leads to compromised endocytosis in cultured neurons (Gareus et al., 2006). It is apparent that, in addition to twinfilin, ADF/cofilin and profilin, the two crucial players in actin filament turnover, are also involved in endocytosis.

In summary, we have shown that *twf* mutants exhibit increased F-actin formation in disparate cellular contexts and defects in different cellular functions, from axonal growth and cell migration to synaptic endocytosis. A common feature of these processes is that they all depend on a highly dynamic actin cytoskeleton. When the function of twinfilin is abolished in these processes, dynamic actin would be turned into a more 'stagnant' state, which is reflected in the increased F-actin formation observed in different cellular contexts. The disruption of actin dynamics in *twf* mutants could compromise endocytosis in NMJ synapses and lamellipodial extension in both growing axons and migrating cells. Thus, our study reveals a crucial in vivo role for twinfilin in promoting actin dynamics, which is essential for a range of cellular processes in both neuronal and non-neuronal systems.

Materials and Methods

Drosophila strains and genetics

Fly cultures were maintained at 25°C unless specified. w^{1118} flies were used as the wild-type control in all experiments. twf^{3701} is a hypomorphic allele of *twf* as previously described (Wahlström et al., 2001). Two *twf* deletion alleles, twf^{110} and twf^{102}, were generated by means of *P*-element-mediated excision from *EP(3)3701* (Fig. 1). *Df(3R)suHw*^{7} (deleting 88A9-B2 carrying *twf*), tsr^{N96A} and $chic^{221}$ were from the Bloomington Stock Center. The *twf* RNAi transgenic stock was obtained from the Vienna *Drosophila* RNAi Center. The *UAS-twf* strain was generated by inserting the full-length ORF of *twf* from the pGAT2 expression vector (Wahlström et al., 2001) into the pUAST vector, followed by germline transformation of the construct into w^{1118} as the host. For targeted knockdown, overexpression or rescue experiments, the tissue-specific Gal4 drivers *elav-Gal4* (pan-neuronal), *OK107-Gal4* (mushroom body), *C57-Gal4* (muscular), *slbo-Gal4* (BCs) and *act-Gal4* (ubiquitous) were used. To obtain *twf* mutant clones in the ovary, *y w*; *FRT82B* twf^{110}*/TM6B* was crossed with *y w hs-Flp*; *FRT82B ubi-GFP/TM3*. All progeny were heat shocked at 37°C, 2 hours a day for 3 days beginning at the second-instar larval stage. Upon eclosion, flies were transferred to fresh food and dissected 3 days later.

Immunochemical analysis

Immunostaining of various tissues was performed essentially as previously described (Zhang et al., 2001; Jin et al., 2009). Specifically, late third-instar larvae were dissected in Ca^{2+}-free standard saline and then fixed in fresh 4% paraformaldehyde for 30 minutes for all NMJ preparations. For GluRIIA and GluRIIB staining, larvae were dissected in saline with 2 mM L-glutamate, followed by ice-cold methanol fixation for 5 minutes. Adult brains were dissected in PBS and then fixed in fresh 4% paraformaldehyde for 40 minutes. Ovaries were dissected in PBS and then fixed in a mixture of devitellinizing buffer (7% formaldehyde) and heptane (Sigma) (1:6) for 10 minutes. The following primary antibodies or reagents were used: FITC-conjugated goat anti-HRP (Jackson ImmunoResearch, 1:100), Texas-Red phalloidin (Molecular Probes, 1:6 for NMJ staining), TRITC phalloidin (Sigma, 1:100 for ovary staining), rabbit anti-GluRIIB (from Aaron DiAntonio, Washington University, WA, 1:2500), rabbit anti-twinfilin (1:2000) (Wahlström et al., 2001) and guinea-pig anti-Coracle (from Richard Fehon, University of Chicago, IL, 1:250). Monoclonal mouse antibodies anti-Dlg (4F3; 1:1000), anti-Fas II (1D4; 1:50) and anti-GluRIIA (1:50) were from the Developmental Studies Hybridoma Bank at the University of Iowa. AlexaFluor-488, -568 or -635-conjugated anti-mouse or anti-rabbit secondary antibodies (Invitrogen; 1:1000) were used. All images were collected using a Leica SP5 laser scanning confocal microscope or an Olympus BX51 fluorescent microscope, and processed with Adobe Photoshop 8.0.

For western blotting, 20 adult heads from each genotype were homogenized in 120 µl common lysis buffer containing 2% SDS on ice. The immunoblots were incubated overnight at 4°C with the following primary antibodies: anti-twinfilin (1:20,000), anti-dAbi (from Sven Bagdan, Wilhelms-University Münster, Germany; 1:1000), anti-α-tubulin (mAb B-5-1-2; Sigma; 1:70,000) and anti-actin (mAb1501; Chemicon; 1:35,000). The secondary antibody HRP-labeled anti-mouse IgG was diluted at 1:20,000 in PBS-Tween containing 5% milk. Protein bands were visualized with HRP chromogenic reagents from Millipore.

Scanning electron microscopy

Scanning electron microscopy (SEM) of bristles was carried out as previously published (Hopmann and Miller, 2003). Briefly, after anaesthetizing with CO_2, adult flies with wings removed and abdomens punctured were transferred to a solution of 25% glycerol in 95% ethanol for at least 2 days. The fixed flies were dehydrated through a graded series of ethanol solutions: 70%, 95% and three times of 100% ethanol for 15 minutes each. The ethanol was then replaced with hexamethyldisilazane with four changes to prevent distortion, followed by drying overnight and sputter coating with gold before phototaking with a Hitachi S-3000N scanning electron microscope. Statistical analysis of bristle length was performed (following Hopmann and Miller, 2003).

FM1-43 uptake assay

For the FM1-43 uptake assay, we followed previously published protocols (Kuromi and Kidokoro, 1998; Dickman et al., 2005). Late third-instar larvae were dissected in a low Ca^{2+} saline and washed with the normal medium (Jan and Jan, 1976). To load the fluorescent FM1-43 dye, membrane depolarization was achieved by incubating the preparations in a high K^+ (90 mM) solution containing 10 µM FM1-43 (Molecular Probes) for 5 minutes. The preparations were vigorously washed three times with Ca^{2+}-free saline for 5 minutes. The loaded synapses were imaged on a Leica SP5 confocal microscope with a 40× water-immersion lens. After imaging, the preparations were rested for 5 minutes and high K^+ saline without FM1-43 was applied again for 5 minutes to elicit exocytosis. To investigate the effect of actin drugs on synaptic vesicle endocytosis, the dissected larval preparations were incubated for 5 minutes with 0.1 or 10 µM LatA, an actin-monomer-sequestering drug, before loading FM1-43. The composition of the normal medium (Jan and Jan, 1976) was as follows: 128 mM NaCl, 35.5 mM sucrose, 2 mM KCl, 4 mM $MgCl_2$, 1.8 mM $CaCl_2$ and 5 mM (pH 7.3) HEPES. For low Ca^{2+} saline, 0.2 mM instead of 1.8 mM Ca^{2+} was added to the normal medium, whereas for Ca^{2+}-free saline, $CaCl_2$ in the normal medium was replaced by 0.5 mM EGTA. High K^+ saline contained 90 mM KCl, whereas NaCl was reduced by an equivalent amount.

Quantification of fluorescence intensity

Image J was used to quantify fluorescence intensities. Antibody staining and the FM1-43 dye uptake assay were repeated at least three times and the different genotypes were processed in the same tube for better comparison. For each channel,

an arbitrary threshold was set and used for all relevant images. The sum of pixel intensities above the threshold was recorded for each channel. The ratio of phalloidin:anti-HRP, anti-GluRIIA:anti-HRP or anti-GluRIIB:anti-HRP staining intensity was calculated for each genotype in Figs 3 and 6. Three individual boutons were analyzed for phalloidin staining quantification per animal (Fig. 3), whereas two or three NMJs in the A2 or A3 segment of each animal were analyzed for GluR staining (Fig. 6) and FM1-43 live imaging (Fig. 7). For comparison of the F-actin level in BCs (Fig. 4), ovaries expressing *UAS-twf* or *twf* siRNA were mixed with the wild-type controls. They were then processed in the same tube and photographed using the same settings. The genotypes were unambiguously identified by the presence or absence of GFP and anti-twinfilin staining. Statistical analysis of fluorescence intensities was performed using the Student's *t*-test.

Quantification of BC migration

Only stage 10 egg chambers were selected and examined for quantification of BC migration. Flies examined for BC migration were raised at 29°C for *twf* overexpression, RNAi knockdown and *twf* mutants or at 25°C for clonal analysis of *twf* mutants. The extent of BC migration is measured as 0% (no migration), <50%, >50% and 100% (reaching the border) for quantitative analyses. Wild-type BCs would have migrated to the 100% position in a stage 10 egg chamber, whereas a migration delay means that the BC cluster fails to migrate to the final 100% position.

Physiological assays

Intracellular recordings were carried out at 20°C, following a conventional procedure (Jan and Jan, 1976; Jin et al., 2009). For the basal transmission assay, wandering third-instar larvae were dissected in Ca^{2+}-free HL3.1 saline (Feng et al., 2004) and recorded in HL3.1 saline containing 0.25 mM Ca^{2+}. Intracellular microelectrodes with a resistance of 8-20 MΩ filled with 3M KCl were used for the assay. Recordings were performed using an Axoclamp 2B amplifier (Axon Instruments) in Bridge mode. Data were filtered at 1 kHz, digitized using Digitizer 1322A (Axon Instruments) and collected with Clampex 9.1 software. EJPs were evoked at 0.3 Hz by a suction electrode with a depolarizing pulse delivered by a Grass S48 stimulator (Astro-Grass Inc.). EJPs were recorded from muscle 6 of abdominal segment A2 or A3, followed by miniature EJP (mEJP) recording for 120 seconds. EJP and mEJP recordings were processed with Clampfit 10.2 software. Quantal content was calculated by dividing the corrected EJP amplitude by the mEJP amplitude according to a classical protocol (Martin, 1955). The EJP correction for nonlinear summation was done using a reversal potential of 10 mV. At least eight animals were recorded for each genotype. For examining synaptic transmission under tetanic stimulation, synapses were stimulated at 10 Hz for 10 minutes and recorded in a modified HL3.1 saline with 10 mM extracellular Ca^{2+} (Dickman et al., 2005).

We thank Vivian Budnik, Sven Bogdan, Richard Fehon, Aaron DiAntonio, the Bloomington Stock Center, the Vienna *Drosophila* RNAi Center and the Developmental Studies Hybridoma Bank, University of Iowa for fly stocks and antibodies. We thank Pekka Lappalainen for comments on the manuscript and Zhihua Liu for advice on electrophysiology. We are grateful to Xing Ma for assistance in the identification of *twf* mutants and analysis of mushroom-body phenotypes. Discussions with David Featherstone and members of our laboratories are acknowledged. This work is supported by grants from the National Science Foundation of China (30430250 and 30525015 to Y.Q.Z.; 30570910 and 90608018 to J.C.), the Ministry of Science and Technology of China (2007CB947200 to Y.Q Z.; 2007CB947101 and 2006CB943503 to J.C.) and the Chinese Academy of Sciences (KSCX1-YW-R-69 to Y.Q.Z.).

Supplementary material available online at
http://jcs.biologists.org/cgi/content/full/123/9/1546/DC1

References

Baum, B. and Perrimon, N. (2001). Spatial control of the actin cytoskeleton in Drosophila epithelial cells. *Nat. Cell Biol.* **3**, 883-890.

Boquet, I., Boujemaa, R., Carlier, M. F. and Preat, T. (2000). Ciboulot regulates actin assembly during Drosophila brain metamorphosis. *Cell* **102**, 797-808.

Chen, J., Godt, D., Gunsalus, K., Kiss, I., Goldberg, M. and Laski, F. A. (2001). Cofilin/ADF is required for cell motility during Drosophila ovary development and oogenesis. *Nat. Cell Biol.* **3**, 204-209.

Chen, K., Merino, C., Sigrist, S. J. and Featherstone, D. E. (2005). The 4.1 protein coracle mediates subunit-selective anchoring of Drosophila glutamate receptors to the postsynaptic actin cytoskeleton. *J. Neurosci.* **25**, 6667-6675.

Cingolani, L. A. and Goda, Y. (2008). Actin in action: the interplay between the actin cytoskeleton and synaptic efficacy. *Nat. Rev. Neurosci.* **9**, 344-356.

Coleman, S. K., Cai, C., Mottershead, D. G., Haapalahti, J. P. and Keinanen, K. (2003). Surface expression of GluR-D AMPA receptor is dependent on an interaction between its C-terminal domain and a 4.1 protein. *J. Neurosci.* **23**, 798-806.

Coyle, I. P., Koh, Y. H., Lee, W. C., Slind, J., Fergestad, T., Littleton, J. T. and Ganetzky, B. (2004). Nervous wreck, an SH3 adaptor protein that interacts with Wsp, regulates synaptic growth in Drosophila. *Neuron.* **41**, 521-534.

DiAntonio, A., Petersen, S. A., Heckmann, M. and Goodman, C. S. (1999). Glutamate receptor expression regulates quantal size and quantal content at the Drosophila neuromuscular junction. *J. Neurosci.* **19**, 3023-3032.

Dickman, D. K., Horne, J. A., Meinertzhagen, I. A. and Schwarz, T. L. (2005). A slowed classical pathway rather than kiss-and-run mediates endocytosis at synapses lacking synaptojanin and endophilin. *Cell* **123**, 521-533.

Dickman, D. K., Lu, Z., Meinertzhagen, I. A. and Schwarz, T. L. (2006). Altered synaptic development and active zone spacing in endocytosis mutants. *Curr. Biol.* **16**, 591-598.

Falck, S., Paavilainen, V. O., Wear, M. A., Grossmann, J. G., Cooper, J. A. and Lappalainen, P. (2004). Biological role and structural mechanism of twinfilin-capping protein interaction. *EMBO J.* **23**, 3010-3019.

Feng, Y., Ueda, A. and Wu, C. F. (2004). A modified minimal hemolymph-like solution, HL3.1, for physiological recordings at the neuromuscular junctions of normal and mutant Drosophila larvae. *J. Neurogenet.* **18**, 377-402.

Gareus, R., Di Nardo, A., Rybin, V. and Witke, W. (2006). Mouse profilin 2 regulates endocytosis and competes with SH3 ligand binding to dynamin 1. *J. Biol. Chem.* **281**, 2803-2811.

Goode, B. L., Drubin, D. G. and Lappalainen, P. (1998). Regulation of the cortical actin cytoskeleton in budding yeast by twinfilin, a ubiquitous actin monomer-sequestering protein. *J. Cell Biol.* **142**, 723-733.

Helfer, E., Nevalainen, E. M., Naumanen, P., Romero, S., Didry, D., Pantaloni, D., Lappalainen, P. and Carlier, M. F. (2006). Mammalian twinfilin sequesters ADP-G-actin and caps filament barbed ends: implications in motility. *EMBO J.* **25**, 1184-1195.

Hopmann, R. and Miller, K. G. (2003). A balance of capping protein and profilin functions is required to regulate actin polymerization in Drosophila bristle. *Mol. Biol. Cell* **14**, 118-228.

Idrissi, F. Z., Wolf, B. L. and Geli, M. I. (2002). Cofilin, but not profilin, is required for myosin-I-induced actin polymerization and the endocytic uptake in yeast. *Mol. Biol. Cell* **13**, 4074-4087.

Iwasa, J. H. and Mullins, R. D. (2007). Spatial and temporal relationships between actin-filament nucleation, capping, and disassembly. *Curr. Biol.* **17**, 395-406.

Jan, L. Y. and Jan, Y. N. (1976). Properties of the larval neuromuscular junction in Drosophila melanogaster. *J. Physiol.* **262**, 189-214.

Jin, S., Pan, L., Liu, Z., Wang, Q., Xu, Z. and Zhang, Y. Q. (2009). Drosophila Tubulin-specific chaperone E functions at neuromuscular synapses and is required for microtubule network formation. *Development* **136**, 1571-1581.

Kaksonen, M., Toret, C. P. and Drubin, D. G. (2006). Harnessing actin dynamics for clathrin-mediated endocytosis. *Nat. Rev. Mol. Cell Biol.* **7**, 404-414.

Koh, T. W., Verstreken, P. and Bellen, H. J. (2004). Dap160/intersectin acts as a stabilizing scaffold required for synaptic development and vesicle endocytosis. *Neuron* **43**, 193-205.

Kuromi, H. and Kidokoro, Y. (1998). Two distinct pools of synaptic vesicles in single presynaptic boutons in a temperature-sensitive Drosophila mutant, shibire. *Neuron* **20**, 917-925.

Lappalainen, P. and Drubin, D. G. (1997). Cofilin promotes rapid actin filament turnover in vivo. *Nature* **388**, 78-82.

Marrus, S. B., Portman, S. L., Allen, M. J., Moffat, K. G. and DiAntonio, A. (2004). Differential localization of glutamate receptor subunits at the Drosophila neuromuscular junction. *J. Neurosci.* **24**, 1406-1415.

Martin, A. R. (1955). A further study of the statistical composition on the end-plate potential. *J. Physiol.* **130**, 114-122.

Michel, C. I., Kraft, R. and Restifo, L. L. (2004). Defective neuronal development in the mushroom bodies of Drosophila fragile X mental retardation 1 mutants. *J. Neurosci.* **24**, 5798-5809.

Moseley, J. B., Okada, K., Balcer, H. I., Kovar, D. R., Pollard, T. D. and Goode, B. L. (2006). Twinfilin is an actin-filament-severing protein and promotes rapid turnover of actin structures in vivo. *J. Cell Sci.* **119**, 1547-1557.

Naora, H. and Montell, D. J. (2005). Ovarian cancer metastasis: integrating insights from disparate model organisms. *Nat. Rev. Cancer* **5**, 355-366.

Ng, J. and Luo, L. (2004). Rho GTPases regulate axon growth through convergent and divergent signaling pathways. *Neuron* **44**, 779-793.

Ojala, P. J., Paavilainen, V. O., Vartiainen, M. K., Tuma, R., Weeds, A. G. and Lappalainen, P. (2002). The two ADF-H domains of twinfilin play functionally distinct roles in interactions with actin monomers. *Mol. Biol. Cell* **13**, 3811-3821.

Okreglak, V. and Drubin, D. G. (2007). Cofilin recruitment and function during actin-mediated endocytosis dictated by actin nucleotide state. *J. Cell Biol.* **178**, 1251-1264.

Paavilainen, V. O., Bertling, E., Falck, S. and Lappalainen, P. (2004). Regulation of cytoskeletal dynamics by actin-monomer-binding proteins. *Trends Cell. Biol.* **14**, 386-394.

Paavilainen, V. O., Hellman, M., Helfer, E., Bovellan, M., Annila, A., Carlier, M. F., Permi, P. and Lappalainen, P. (2007). Structural basis and evolutionary origin of actin filament capping by twinfilin. *Proc. Natl. Acad. Sci. USA* **104**, 3113-3118.

Palmgren, S., Ojala, P. J., Wear, M. A., Cooper, J. A. and Lappalainen, P. (2001). Interactions with PIP2, ADP-actin monomers, and capping protein regulate the activity and localization of yeast twinfilin. *J. Cell Biol.* **155**, 251-260.

Palmgren, S., Vartiainen, M. and Lappalainen, P. (2002). Twinfilin, a molecular mailman for actin monomers. *J. Cell Sci.* **115**, 881-886.

Pantaloni, D., Le Clainche, C. and Carlier, M. F. (2001). Mechanism of actin-based motility. *Science* **292**, 1502-1506.

Pelkmans, L., Fava, E., Grabner, H., Hannus, M., Habermann, B., Krausz, E. and Zerial, M. (2005). Genome-wide analysis of human kinases in clathrin- and caveolae/raft-mediated endocytosis. *Nature* **436**, 78-86.

Rosenmund, C. and Westbrook, G. L. (1993). Calcium-induced actin depolymerization reduces NMDA channel activity. *Neuron* **10**, 805-814.

Schenck, A., Bardoni, B., Langmann, C., Harden, N., Mandel, J. L. and Giangrande, A. (2003). CYFIP/Sra-1 controls neuronal connectivity in Drosophila and links the Rac1 GTPase pathway to the fragile X protein. *Neuron* **38**, 887-898.

Shirao, T. and Sekino, Y. (2001). Clustering and anchoring mechanisms of molecular constituents of postsynaptic scaffolds in dendritic spines. *Neurosci. Res.* **40**, 1-7.

Smythe, E. and Ayscough, K. R. (2006). Actin regulation in endocytosis. *J. Cell Sci.* **119**, 4589-4598.

Vartiainen, M., Ojala, P. J., Auvinen, P., Peranen, J. and Lappalainen, P. (2000). Mouse A6/twinfilin is an actin monomer-binding protein that localizes to the regions of rapid actin dynamics. *Mol. Cell. Biol.* **20**, 1772-1783.

Vartiainen, M. K., Sarkkinen, E. M., Matilainen, T., Salminen, M. and Lappalainen, P. (2003). Mammals have two twinfilin isoforms whose subcellular localizations and tissue distributions are differentially regulated. *J. Biol. Chem.* **278**, 34347-34355.

Verstreken, P., Kjaerulff, O., Lloyd, T. E., Atkinson, R., Zhou, Y., Meinertzhagen, I. A. and Bellen, H. J. (2002). Endophilin mutations block clathrin-mediated endocytosis but not neurotransmitter release. *Cell* **109**, 101-112.

Wahlström, G., Vartiainen, M., Yamamoto, L., Mattila, P. K., Lappalainen, P. and Heino, T. I. (2001). Twinfilin is required for actin-dependent developmental processes in Drosophila. *J. Cell Biol.* **155**, 787-796.

Winder, S. J. and Ayscough, K. R. (2005). Actin-binding proteins. *J. Cell Sci.* **118**, 651-654.

Wolven, A. K., Belmont, L. D., Mahoney, N. M., Almo, S. C. and Drubin, D. G. (2000). In vivo importance of actin nucleotide exchange catalyzed by profilin. *J. Cell Biol.* **150**, 895-904.

Zhang, Y. Q., Bailey, A. M., Matthies, H. J., Renden, R. B., Smith, M. A., Speese, S. D., Rubin, G. M. and Broadie, K. (2001). Drosophila fragile X-related gene regulates the MAP1B homolog Futsch to control synaptic structure and function. *Cell* **107**, 591-603.